Article

Greatly enhanced photovoltaic performance of crystalline silicon solar cells using metal oxide layers by band-gap alignment engineering

Lingling Zhou[1], Lufei Xiao[1], Hai Yang[2], Jie Liu[2,*] and Xibin Yu[2,*]

[1] Department of Food and Environmental Engineering, Chuzhou Vocational and Technical College, Chuzhou 239000, P. R. China. E-mail: zhoulingling2003@126.com (L. Z.); xlf3345@163.com (L.X.)

[2] The Education Ministry Key Laboratory of Resource Chemistry and Shanghai Key Laboratory of Rare Earth Functional Materials, Department of Chemistry, Shanghai Normal University, Shanghai 200234, P. R. China.

* Correspondence: E-mail: liujie@shnu.edu.cn; xibinyu@shnu.edu.cn; Tel.: +86-21-64324528

Abstract: Band-gap alignment engineering has now been extensively studied due to its high potential application. Here we demonstrate a simple route to synthesize two metal oxide layers and align them together according to their bandgaps on surface of crystalline silicon(c-Si) solar cells. The metal oxide layers can not only extend absorption spectrum to generate extra carriers but also serve to separate electron-hole pairs more efficiently. As a consequence, the photovoltaic performance of SnO_2/CdO /Si double-layer solar cell (DLSC) is highly improved compared to CdO/Si and SnO_2/Si single-layer solar cells(SLSCs) and SnO_2/CdO/Si double-layer solar cell(DLSC). By the alignment engineering, the SnO_2/CdO/Si DLSC produces a short circuit photocurrent (J_{sc}) of 38.20 mA/cm^2, an open circuit photovoltage (V_{oc}) of 0.575 V and a fill factor (FF) of 68.7%, corresponding to a light to electric power conversion efficiency (η) of 15.09% under AM1.5 illumination. These results suggest that with the use of metal oxide layers by band-gap alignment engineering, new avenues have been opened for developing high-efficiency and cost-effective c-Si solar cells.

Keywords: silicon solar cells; semiconductors; electron-hole pairs

1. Introduction

Solar cells have now been developed for more than five decades. F- rom the very first generation solar cell to the latest one ,the conve- rsion efficiency of solar cell itself has been largely improved. The update conversion efficiency of GaInP/GaAs solar cells have broken 40%[1-4]. However, these high efficiency solar cells still have many disadvantages, such as stability issue and high cost, so that they can hardly be put into large-scale production. At this point, with the combination of high purity, natural abundance, a matching insulator and maturity of production[5,6], crystalline silicon (c-Si) solar cells show their unique advantageous properties. But still, there are several defects of c-Si solar cells, such as optical loss, recombination and thermal or quantum losses[7]. Among them, optical loss and recombination are deemed to be two most vital factors. Yet many efforts have been made by researchers to solve these problems. Silicon nanowires[8-10], ZnO nanowires[11], and CuO nanoleaves[12], are some of those extraordinary attempts. The power conversion efficiency has been improved through light trapping enhancement and photocarrier collection facilitation[13-14]. It has opened up new opportunities to achieve higher energy conversion efficiency at lower fabrication costs.

Although many textured structures have been made to enhance absorptance of c-Si solar cells, c-Si is still an indirect band-gap semiconductor with a bandgap of 1.12eV, which is able to utilize only a small fraction of the solar spectrum. Currently, tandem solar cell is considered to be one of the most promising approaches of the third generation solar cells to solve this problem. It is fabricated with more than one sub cells which are tandemed according to their bandgaps[15-16]. It is reported that the overall open circuit voltage (*V*oc) is the sum of

Preprints (www.preprints.org) | NOT PEER-REVIEWED | Posted: 27 April 2018 doi:10.20944/preprints201804.0353.v1

those from all individual sub-cells, while the current is the same as that in a single sub-cell once their currents are matched[17-19]. As a result, tandem solar cell has broadened absorption spectrum effectively, so that it can tackle simultaneously absorption and thermalization losses by absorbing the higher energy photons and finally improve conversion performance.

By using the concept of tandem solar cells for reference, band-gap alignment engineering has been developed for various applications, such as quantum dot solar cells through band alignment engineering[20]. Here we applied CdO and SnO_2 semiconductors to c-Si solar cells. CdO is one of the transparent conducting oxides(TCOs) that has both, moderate band-gap and high electrical conductivity. With high mobility, CdO is also believed to have large potential for the use in active electronic devices[21-22]. SnO_2 nanostructures are always applied to gas sensor and photocatalysis[23]. Besides, with wide bandgap of 3.5~4.0eV and terrific electronic conductivity, it is believed to have a great prospect in solar cells. Herein, in our research we have tried to synthesize different nano−structured films of CdO and SnO_2 semiconductors on surface of c-Si substrate respectively. To investigate electrical properties and photovoltaic performance, we compared as-synthesized solar cells with CdO single layer to cells with SnO_2 single layer and cells with CdO layer and SnO_2 layer stacked together in the order of their bandgaps. CdO/Si single-layer solar cell (SLSC) and SnO_2/Si single layer solar cell were produced with chemical bath deposition and spin-coating method after which a certain temperature thermal treatment was conducted to form oxide layers. Two steps of thermal treatment were included in synthesis of SnO_2/CdO/Si double-layer solar cell (DLSC) to confirm a firm contact between double layers and the Si substrate. It is found that the characteristics of SnO_2/CdO/Si DLSC offer broad-band light harvesting and super high minority carrier lifetime. Here we compare two SLSCs to SnO_2/CdO/Si DLSC to demonstrate the impact of different layers with different bandgaps on absorption region and charge-transfer efficiency. As a result, the short-circuit current (*J*sc) and the open circuit voltage were improved which led to the enhancement of power conversion efficiency (PCE). We believe that the cost effective technology can be easily applied to the industrial scale production of Si solar cells.

2. Materials and Methods

Synthetic prcedures

Slices (3.0×3.0 cm^2) of c-Si wafers without Si_3N_4 antireflection layer were applied in this work.The thickness of wafers is ~200μmwith a bulk *p–n* junction. Before growing any filmon the surface of Si wafer was first cleaned by rinsing with double distilled water and ethanolto eliminate any impurities. Firstly, two depositing solutions were prepared as solution A and B. Solution A was composed by 0.05M Cadmium acetate dihydrate [$Cd(CH_3COO)_2.H_2O$] and double distilled water. In solution B, 0.01M Stannic chloride pentahydrate aqueous was mixed with ethanol to prohibitthe solution from hydrolyzing. In order to grow CdO single layer on surface of Si wafers, dried Si wafer was immersed in solution A for 2mins and was dried again in drying oven under the temperature of 80°C. This procedure then was repeated for four more times to ensure the CdO seeds were fully distributed on the silicon's surface before sending the deposited Si wafer into muffle furnace. After thermal treatment of 500°C for 3 mins, the CdO/Si SLSC was completed. SnO_2/Si SLSC was synthesized by spin-coating method. In this tep, firstly, 0.05 mL of 0.01M Stannic chloride pentahydrate aqueous ethanol solution were dropped onto Si surface under the speed of 1500 rpm for 40s, and 5 times ofthis operation were needed to ensure the Sn-precursor got the substrate full covered. Finally the deposited Si wafer was treated under 900°C in muffle furnace for 5 mins to form SnO_2 film. With combination of two procedures above, SnO_2 seed solution was deposited on surface of as-synthesied CdO/Si composited cell and 900°C annealing treatment was also conducted.

Characterization

Field emission scanning electron microscopic (FESEM, HitachiS-4800) was used to observe the morphology of the layers. The minority carrier lifetime of the samples are measured using the Si wafer life-timeSEMILAB WT-2000 PVN. The current density–voltage (*J–V*) characteristics of the solar cells are measured using an electrochemical workstation (Zahner, Zennium) under 100 $mW \times cm^{-2}$ calibration which is performed using a Class A AM 1.5G spectral distributed Abet Technologies Sun 2000 Solar Simulator.

Preprints (www.preprints.org) | NOT PEER-REVIEWED | Posted: 27 April 2018 doi:10.20944/preprints201804.0353.v1

3. Results and discussion

Fig. 1 shows the surface morphologies of both CdO and SnO_2 films growing on the surface of polycrystalline silicon with p-n junction respectively. As shown in Fig. 1 (a), CdO film was characterized by Scanning Electron Microscope (SEM). The cross-section view indicates that the thickness of the film is about 32nm, and the surface of it is smooth with comparison of top view picture. While in Figure 1 (b), SnO_2 film shows a different surface morphology with many hollows on it, and it is approximately 41nm in thickness which is slightly thicker than CdO film. With those pictures we can find that both of two films have a firm contact with Si substrates, which is beneficial to reduce contact resistance and electron transfer. Fig. 1(c) demonstrates the schematic of SnO_2/CdO/Si DLSC. With spin-coating method and annealing treatments, CdO layer and SnO_2 layer were grown on Si substrate in sequence. On one hand, the top layer with rough surface of SnO_2 can efficiently increase light trapping. On the other hand, two layers are capable to utilize different region of incident light which is believed to contributed to considerable enhancement of photovoltaic performance.

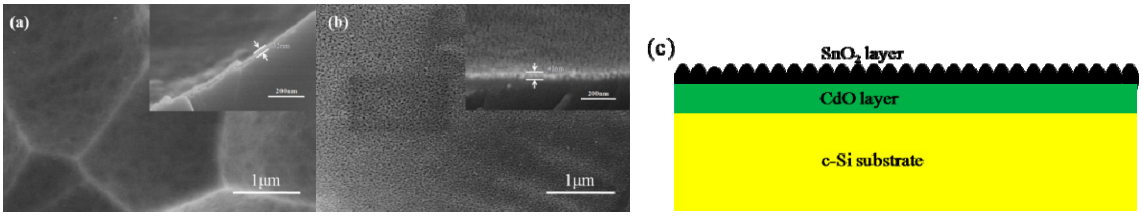

Figure 1. Cross-section and top views of SEM morphologies of (a) CdO; and (b) SnO_2films growing on polycrystalline silicon substrates respectively; (c) Schematic of SnO_2/CdO/Si DLSC.

FESEM energy dispersive spectrometry (EDS) element mapping of composited SnO_2/CdO/Si DLSC was conducted to take deep research on the structure of layer-by-layer. As we can see in Fig. 2, (a) is the scanning region of SnO_2/CdO/Si composited wafer, while Fig 2 (b) is mapping of all detected elements. Fig. 2 (c)~Fig. 2 (f) refer to element Si, O, Sn and Cd respectively. From Fig. 2 (c) to Fig. 2 (f) we can find that the elements are well-distributed on the surface of c-Si substrate which indicates that the layer-by-layer structure was greatly formed by spin-coating and annealing procedures.

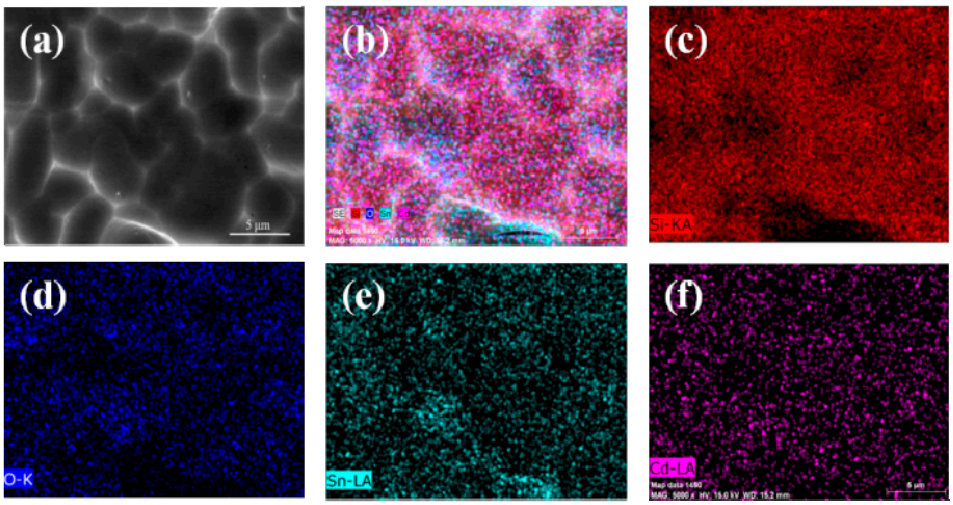

Figure 2. FESEM-EDS element mapping of the composited SnO_2/CdO/Si DLSC.

According to different morphologies above, different absorption spectra were measured by UV-vis-IR. In Fig. 3, Si substrate with CdO layer shows almost the same absorption property as Si wafer except the slight improvement between 300-450nm. But as to SnO_2 layer, from 300-1100 nm the absorption value is improved by about 16%. The reason contributed to this phenomenon is that the difference of surface structures. With hollows on surface, the film can cause optical resonance

Preprints (www.preprints.org) | NOT PEER-REVIEWED | Posted: 27 April 2018 doi:10.20944/preprints201804.0353.v1

and multiple scattering of the incident light, which can trap incident light and enhance absorptance effectively[24-26]. In addition, due to its wide bandgap SnO_2 film is capable to utilize much more light compared to c-Si wafer.

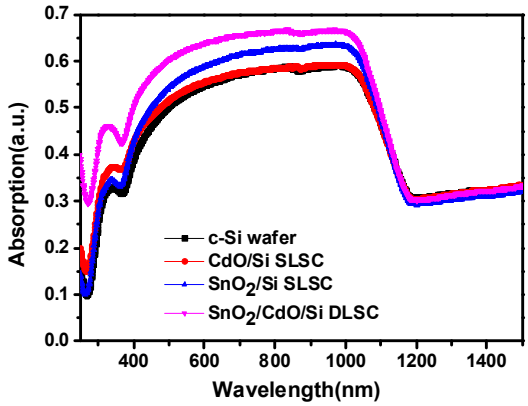

Figure 3. UV-vis-IR absorption spectra for CdO/Si and SnO_2/Si SLSCs and SnO_2/CdO/Si DLSC.

To further investigate photovoltaic properties of composited solar cells, External Quantum Efficiency(EQE) spectra and J-V curves were conducted under the standard AM 1.5G conditions. Fig. 4 (a) shows that a broad value of 70% ~ 80% in the spectrum of pristine Si solar cell is observed from 500~900nm which corresponds to the wavelength range of Si light absorption. In contrast, the spectrum of SnO_2/Si SLSC exhibits a large increase in EQE spectrum for the wavelength between 300~550nm, while CdO/Si SLSC is a little low than that of SnO_2/Si SLSC.On one hand, as two semiconductors with wide bandgap (Eg_{CdO} =2.4eV , Eg_{SnO2}=3.5eV), CdO and SnO_2 can effectively absorb spectrum wavelength between 250~600nm. That means the CdO layer and SnO_2 layer are able to use incident light from 250~600nm and generate more carrier with high energy while c-Si can not. On the other hand, according to UV-vis-IR absorption spectra, both CdO/Si SLSC and SnO_2/Si SLSC have been enhanced between 300-500nm. As we know, if solar cells absorb more incident light, more photons can be utilized to generate carriers. So the improve- ment of EQE can be also attributed to the enhancement of absorption performance. Finally, the EQE performance of SnO_2/CdO/Si DLSC matches the theory we discussed above as well.

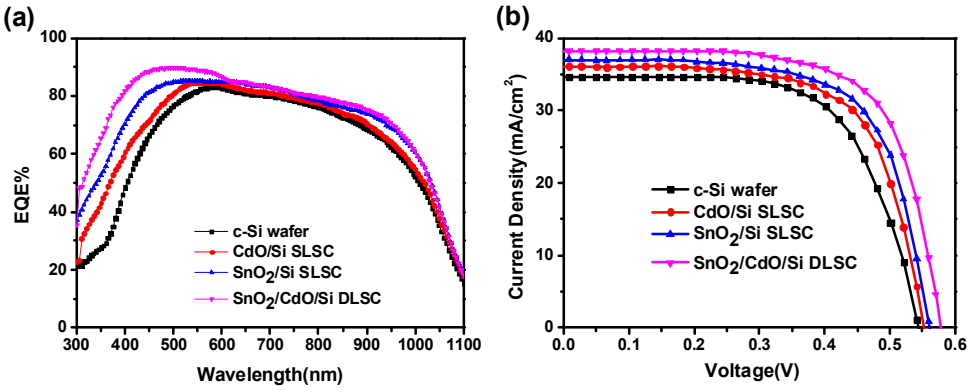

Figure 4. (a) External Quantum Efficiency (EQE) spectra and (b) *J-V* characteristics for CdO/Si and SnO_2/Si SLSCs and SnO_2/CdO/Si DLSC.

The detailed device performance is summarized in Table 1 and the*J-V* characteristic curves are shown in Figure 4 (b). As a result, the PCE of CdO/Si SLSC reaches a value as high as 13.34%, with J_{sc} of 36.12 mA cm^{-2}, V_{OC} of 0.556V and FF of 66.42%, while values of SnO_2/Si SLSC are 13.96%, 37.01mA cm-2, 66.76% respectively. Compared to pristine Si solar cell without any metal oxide film growing on the top, the *V*oc performance are improved by 2.6% and 4.2%. Whereas as to current density, three as-synthesized solar cells all have various increases compared to blank Si solar cell. The

Preprints (www.preprints.org) | NOT PEER-REVIEWED | Posted: 27 April 2018 doi:10.20944/preprints201804.0353.v1

short-circuit current are mainly related with three factors as we concluded, and the very first one is light absorption. The photoactive layer in the solar device absorbs sun light, raising an electron from the ground state to a higher energy state and then generates an energy bearing electron–hole pair, called an excition[27]. As we know, c-Si is a indirect band-gap semi- conductor with a band-gap of 1.12eV and the perfect light spectra region for absorption of c-Si is approximately 700~1100 nm which is only a small part of the whole solar spectrum. So to make full use of the solar spectrum in order to maximize J_{sc}, light-absorbing substance is now fully used. As the more solar spectrum is utilized, the more photo-generated carriers are produced. But a large part of these photo-generated carriers are wasted directly through recombination. It indicates that if electron-hole pairs can be efficiently separated before recombination, J_{sc} value is supposed to be enhanced to a large extend. In addition, to ensure an efficient collection of charge carriers, carriertransporting layers are required to have high mobility as well aslong diffusion lengths for electrons and holes[28-30], and the resistance is also a factor that changes current flowing. In our research, J_{sc} of CdO/Si and SnO_2/Si solar cells are increased to 36.12mA cm^{-2} and 37.01mA cm^{-2}. The increasement can be ascribed to absorption enhancement as shown in Fig. 3 (a) and charge carrier lifetime increase shown in Fig. 5.

Table 1 Photovoltaic performance parameters of blank c-Si solar cell and as-synthesized CdO/Si and SnO_2/Si SLSCs and SnO_2/CdO/Si DLSC.

	V_{oc}[V]	J_{sc}[mA cm^{-2}]	FF[%]	η [%]	Δη[%]
c-Si	0.542	34.68	65.33	12.28	--
CdO/Si	0.556	36.12	66.42	13.34	8.6
SnO_2/Si	0.565	37.01	66.76	13.96	13.6
SnO_2/CdO/Si	0.575	38.20	68.70	15.09	22.8

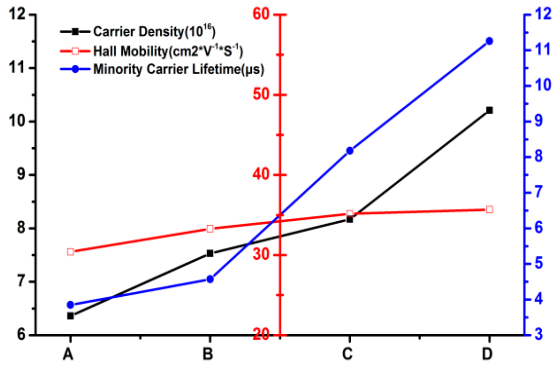

Figure 5. Carrier density, Hall mobility and minority carrier lifetime properties of A (c-Si solar cell), B (CdO/Si SLSC),C (SnO_2/Si SLSC) and D (SnO_2/CdO/Si DLSC).

In Fig. 5 we can also find that carrier density values of three kinds of as-synthesized solar cells are all enhanced. As we discussed above, because of good solar spectrum absorption property and band-gap alignment engineering, the composited solar cells are able to make better use of solar spectra and thus produce more photo-generated carriers. Carrier density is a important parameter to measure the utilized efficiency of absorbed photons. For CdO owns a wider bandgap than c-Si, spectrum region of short wavelength is fully used according to results of UV-vis-IR absorption and EQE property shown in Fig. 3. For the same reason, as bandgap of SnO_2 is even wider, the EQE and UV-vis-IR results indicate the enhancement of carrier density which is correspondence with that measured in Fig. 5. Moreover, Hall mobility is highly related to electrical conductivity. The result in Fig. 5 (red line) shows that with CdO layer and SnO_2 layer growing on top of c-Si substrates, the speed of carrier transport is not decayed but improved instead. This phenomenon demonstrates that CdO layer and SnO_2 layer we have synthesized play a role as good electron transport layers. When CdO and SnO_2 were made to grow on surface of c-Si substrates by spin coating method, homogeneous films were produced through tuning spinning speed and coating time. After

Preprints (www.preprints.org) | NOT PEER-REVIEWED | Posted: 27 April 2018 doi:10.20944/preprints201804.0353.v1

annealing at 500 °C and 900 °C orderly, thin oxide films then were formed with a firm Ohmic contact with c-Si substrates which is supposed to decrease series resistance. Besides, blue line is put to demonstrate the change of minority carrier lifetime., and the result shows that after covered by different oxide layers, lifetime of minority carrier is highly increased. The effective carrier lifetime (τ_{eff}) is directly related to bulk lifetime (τ_{bulk}) and surfacelifetime (τ_{surf}) and the τ_{bulk} dominates the τ_{eff}[31].The increase in JSC and VOC partly contributed byimproved minority carrier lifetime can be understood by the relations below[32].

$$Voc = \frac{kt}{q}\ln\left(\frac{\Delta n(N_{D,A}+\Delta n)}{n_i^2}\right) \quad (1)$$

$$Jsc = qG(L_n + L_p) \quad (2)$$

where (kT)/q is the thermal voltage, $N_{D,A}$ is the donor or acceptor concentration of the wafer, Δn is the excess carrier concentration, n_i is the intrinsic carrier concentration, q is the magnitude of the electrical charge on the electron, G is the generation rate, and L_n and L_p are electron and hole diffusion lengths, respectively. We can find that V_{OC} and J_{SC} strongly depend on excess carrier concentration and diffusion lengths which are directly proportional to the τ_{eff}.That is to say, the increase of minority carrier lifetime gives rise to the enhancement of J_{SC} and V_{OC} and which in the end contribute to power conversion efficiency.

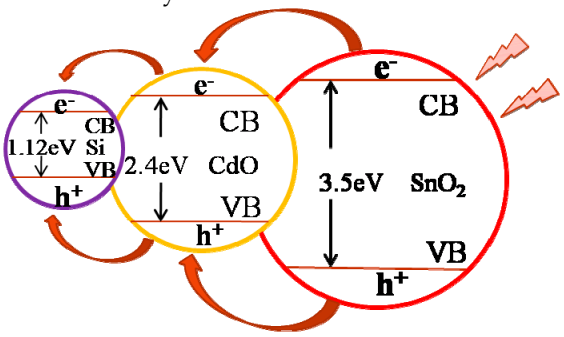

Scheme 1 Schematic diagram representing the charge-transfer and electron-hole separation process in SnO_2/CdO/Si DLSC.

To further investigate the mechanism of charge-transfer and electron-hole separation, we here illustrate the schematic diagram representing charge-transfer and electron-hole separation process in Scheme 1. As shown in the diagram, the conduction band (CB) of SnO_2 lies at a more negative potential than that of CdO, while the valence band (VB) of CdO is more negative than that of SnO_2. Under solar irradiation, photo-generated electrons in the conduction band of SnO_2 go to the conduction band of CdO and hole transfer occurs from the valence band of CdO to that of SnO_2. At the same time, with a similar reason for c-Si substrate, electrons from conduction band of CdO transfer to that of c-Si and holes transfer from valence band of CdO to that of c-Si.The simultaneous transfer of electronsand holes in SnO_2/CdO/Si system increase both the yield andthe lifetime of charge carriers by separating the photo-induced electrons and reducing charge recombination in electron-transfer process[33]. In our research, the results of minority carrier lifetime, carrier density and short current density are able to perfectly support the schematic diagram we discussed above.

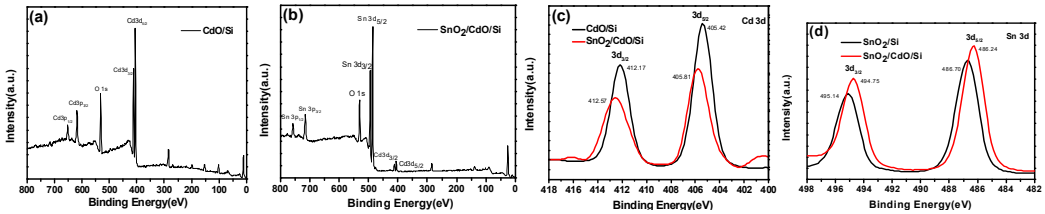

Fig. 6 XPS survey spectra of (a) CdO/Si SLSC and (b) composited SnO_2/CdO/Si DLSC. Core level (c) Cd 3d, (d) Sn 3d XPS spectra.

X-ray photoelectron spectroscopy (XPS) was also conducted tostudy the compositions and chemical states of as-synthesized SnO_2/CdO/Si composited solar cell. Fig.6 (a), (b) compare the XPS survey spectrum of CdO/Si and SnO_2/CdO/Si. In comparison to CdO/Si, the XPS survey spectrum of SnO_2/CdO/Si exhibits four additional Sn peaks, and two strongest peaks refer to Sn $3d_{3/2}$and Sn $3d_{5/2}$. When focusing on Cd 3d, we can find that peaks of Cd 3d in Fig. 6 (b) are apparently much weaker than that in Figure 6 (a). Because of a ~40nm thickness SnO_2 layer covered on top of CdO layer with spin-coating method, XPS signal of Cd was heavily blocked by SnO_2 layer. The Cd 3d core level spectra of CdO/Si solar cell and SnO_2/CdO/Si solar cell are shown in Fig. 6 (c). For CdO/Si, peaks of Cd 3d center at 405.42eV and 412.17eV which are consistent with the values reported for Cd^{2+}, while peaks of Cd $3d_{5/2}$ and Cd $3d_{3/2}$ are located at 405.81eV and 412.57eV respectively for SnO_2/CdO/Si solar cell[34]. There is about a 0.4eV increasement in binding energy of Cd 3d between CdO/Si and SnO_2/CdO/Si, which illustrates that the extraction of nuclei and electrons becomes stronger. It is believed that SnO_2 crystalline and CdO crystalline are affected by each other and formed a kind of hetero-structure. This new formation of structure gives a vital impact on carrier-transport between different layers and also leads to a drastic improvement in the photovoltaic performance of SnO_2/CdO/Si DLSC.

4. Conclusions

In conclusion, we investigated the photovoltaic performance of crystalline silicon solar cells using different metal oxide layers by band-gap alignment engineering that act as wavelength broadening layers for optical absorption and effective carrier separation and transport layers. The photovoltaic performance of as-synthesied SnO_2/Si SLSC, CdO/Si SLSC and SnO_2/CdO/Si DLSC were considerably improved in comparison with original c-Si solar cells. The highest PCE value was 15.09% for SnO_2/CdO/Si DLSC as measured while 12.28% for original c-Si solar cells. In addition, the recombination of photogenerated carriers were greatly restrained, resulting in a high minority carrier lifetime value. It is believed that by using band-gap alignment engineering, crystalline silicon solar cells still have deeper potential for further exploration.

Acknowledgments: This study is supported by the Key Project of Excellent Youth Talent Support Plan of Anhui Province (gxyqZD2016540), Natural Science Foundation of Education Department of Anhui Province (KJ2017ZD49), Talent Project of the College (ZD2017004) and PCSIRT (IRT_16R49).

Author Contributions: Lingling Zhou performed the experiments, analyzed the data and wrote the paper; Lufei Xiao analyzed the data; Hai Yang performed the experiments, analyzed the data and revised the paper; Jie Liu conceived, designed the experiments and revised the paper; Xibin Yu conceived and designed the experiments.

Conflicts of Interest: The authors declare no conflicts of interest.

References

1. Cotal, H.; Fetzer, C.; Boisvert, J.; Kinsey, G.; King, R.; Hebert, P.; Yoon, H.; Karam, N. III–V multijunction solar cells for concentrating photovoltaics. *Energy Environ. Sci.* 2009, **2**, 174-192, DOI: 10.1039/B809257E.
2. Bertness, K. A.; Kurtz, S. R.; Friedman, D. J.; Kibbler, A. E.; Kramer, C.; Olson, J. M. 29.5%-efficient GalnP/GaAs tandem solar cells. *Appl. Phys. Lett.* 1994, **65**, 989-991, DOI: 10.1063/1.112171.
3. Yamaguchi, M.; Takamoto, T.; Araki, K.; Ekins-Daukes N. Multi-junction III–V solar cells: current status and future potential. *Solar Energy*. 2005, **79**, 78-85, DOI: 10.1016/j.solener.2004.09.018.
4. Siddiki, M. K.; Li, J.; Galipeau, D.; Qiao, Q. A review of polymer multijunction solar cells. *Energy Environ. Sci.* 2010, **3**, 867-883, DOI: 10.1039/b926255p.
5. Priolo, F.; Gregorkiewicz, T.; Galli, M.; Krauss, T. F.; *Nature Nanotech*. 2014, **9**, 19-32, DOI: 10.1038/nnano.2013.271.

6. Tisdale, W. A.; Williams, K. J.; Timp, B. A.; Norris, D. J.; Aydil, E. S.; Zhu X. Y. Hot-electron transfer from semiconductor nanocrystals. *Science* 2010, **328**, 1543-1547, DOI: 10.1126/science.1185509.
7. Green, M. A. Solar cells: Operating Principles, Technology and System Applications. The University of New South Wales, Sydney, Australia, 1998.
8. Wang, X.; Peng, K. Q.; Pan, X. J.; Chen, X.; Yang, Y.; Li, L.; Meng, X. M.; Zhang, W. J.; Lee, S. T. High-performance silicon nanowire array photoelectrochemical solar cells through surface passivation and modification. *Angew. Chem., Int. Ed*. 2011, **50**, 9861-9865, DOI: 10.1002/anie.201104102.
9. Garnett, E.; Yang, P. Light trapping in silicon nanowire solar cells. *Nano Lett.* 2010, **10**, 1082-1087, DOI: 10.1021/nl100161z.
10. Peng, K. Q.; Lee, S. T. Silicon nanowires for photovoltaic solar energy conversion. *Adv. Mater.* 2011, **23**, 198-215, DOI: 10.1002/adma.201002410.
11. Pudasaini, P. R.; Ruiz-Zepeda, F.; Sharma, M.; Elam, D.; Ponce, A.; Ayon, A. A. High efficiency hybrid silicon nanopillar-polymer solar cells. *ACS Appl. Mater. Interfaces* 2013, **5**, 9620-9627, DOI: 10.1021/am402598j.
12. Xia, Y. S.; Pu, X. X.; Liu, J.; Liang, J.; Liu, P. J.; Li, X. Q.; Yu, X. B. CuO nanoleaves enhance the c-Si solar cell efficiency. *J. Mater. Chem. A* 2014, **2**, 6796-6800, DOI: 10.1039/C4TA00097H.
13. Ferry, V. E.; Verschuuren, M. A.; Lare, M. C.; Schropp, R. E. I.; Atwater, H. A.; Polman, A. Optimized spatial correlations for broadband light trapping nanopatterns in high efficiency ultrathin film a-Si:H solar cells. *Nano Lett.* 2011, **11**, 4239-4245, DOI: 10.1021/nl202226r.
14. Wang, K. X.; Yu, Z.; Liu, V.; Cui, Y.; Fan, S. Absorption enhancement in ultrathin crystalline silicon solar cells with antireflection and light-trapping nanocone gratings. *Nano Lett*. 2012, 12, 1616-1619, DOI: 10.1021/nl204550q.
15. Yu, R.; Lin, Q.; Leung, S.-F.; Fan, Z. Nanomaterials and nanostructures for efficient light absorption and photovoltaics. *Nano Energy*. 2012, **1**, 57-72, DOI: 10.1016/j.nanoen.2011.10.002.
16. Eisler, C. N.; Abrams, Z. R.; Sheldon, M. T.; Zhang, X.; Atwater, H. A. Multijunction solar cell efficiencies: effect of spectral window, optical environment and radiative coupling. *Energy Environ. Sci.* 2014, **7**, 3600-3605, DOI: 10.1039/C4EE01060D.
17. Ameri, T.; Dennler, G.; Lungenschmied, C.; Brabec, C. J. Organic tandem solar cells: A review. *Energy Environ. Sci.* 2009, **2**, 347-363, DOI: 10.1039/B817952B.
18. Dou, L.; You, J.; Yang, J.; Chen, C.-C.; He, Y.; Murase, S.; Moriarty, T.; Emery, K.; Li, G.; Yang, Y. Tandem polymer solar cells featuring a spectrally matched low-bandgap polymer. *Nature Photon.* 2012, **6**, 180-185, DOI: 10.1038/nphoton.2011.356.
19. Gilot, J.; Wienk, M. M.; Janssen, René A. J. Double and triple junction polymer solar cells processed from solution. *Appl. Phys. Lett.* 2007, **90**, 143512, DOI: 10.1063/1.2719668.
20. Dennler, G.; Scharber, M. C.; Brabec, C. J. Polymer-fullerene bulk-heterojunction solar cells. *Adv. Mater.* 2009, **21**, 1323-1338, DOI: 10.1002/adma.200801283.
21. Chuang, C.-H. M.; Brown, P. R.; Bulović, V.; Bawendi, M. G. Improved performance and stability in quantum dot solar cells through band alignment engineering. *Nat. Mater.* 2014, **13**, 796-801, DOI: 10.1038/nmat3984.

22. Saha, B.; Thapa, R.; Chattopadhyay, K. K. Bandgap widening in highly conducting CdO thin film by Ti incorporation through radio frequency magnetron sputtering technique. *Solid State Commun.* 2008, **145**, 33-37, DOI: 10.1016/j.ssc.2007.10.001.
23. Ueda, N.; Maeda, H.; Hosono, H.; Kawazoe, H. Band-gap widening of CdO thin films. *J. Appl. Phys.* 1998, **84**, 6174-6177, DOI: 10.1063/1.368933.
24. Wang, H. P.; Lien, D. H.; Tsai, M. L.; Lin, C. A.; Chang, H. C.; Lai, K. Y.; He, J. H. Photon management in nanostructured solar cells. *J. Mater. Chem. C* 2014, **2**, 3144-3171, DOI: 10.1039/C3TC32067G.
25. Liu, X. G.; Coxon, P. R.; Peters, M.; Hoex, B.; Cole, J. M.; Fray, D. J. Black silicon: fabrication methods, properties and solar energy applications. *Energy Environ. Sci.* 2014, **7**, 3223-3263, DOI: 10.1039/c4ee01152j.
26. Chen, G. Y.; Seo, J. W.; Yang, C. H.; Prasad, P. N. Nanochemistry and nanomaterials for photovoltaics. *Chem. Soc. Rev.* 2013, **42**, 8304-8338, DOI: 10.1039/C3CS60054H.
27. Zhuang, X. J.; Ning, C. Z.; Pan, A. Composition and bandgap-graded semiconductor alloy nanowires. *Adv. Mater.* 2012, **24**, 13-33, DOI: 10.1002/adma.201103191.
28. Xie, C.; Zhang, X.; Ruan, K.; Shao, Z.; Dhaliwal, S. S.; Wang, L.; Zhang, Q.; Zhang, X.; Jie, J. High-efficiency, air stable graphene/Si micro-hole array Schottky junction solar cells. *J. Mater. Chem. A.* 2013, **1**, 15348-15354, DOI: 10.1039/C3TA13750C.
29. Baek, S. H.; Kim, S.-B.; Shin, J. K.; Kim, J. H. Preparation of hybrid silicon wire and planar solar cells having ZnO antireflection coating by all-solution processes. *Sol. Energy Mater. Sol. Cells*. 2012, **96**, 251-256, DOI: 10.1016/j.solmat.2011.10.007.
30. Polman, A.; Atwater, H. A. Photonic design principles for ultrahigh-efficiency photovoltaics. *Nat. Mater*. 2012, **11**, 174-177, DOI: 10.1038/nmat3263.
31. Sinton, R. A.; Cuevas, A. Contactless determination of current–voltage characteristics and minority-carrier lifetimes in semiconductors from quasi-steady-state photoconductance data. *Appl. Phys. Lett.* 1996, **69**, 2510-2512, DOI: 10.1063/1.117723.
32. Wang, H. P.; Lin, T. Y.; Tsai, M. L.; Tu, W. C.; Huang, M. Y.; Liu, C. W.; Chueh, Y. L.; He, J. H. Toward efficient and omnidirectional n-type Si solar cells: concurrent improvement in optical and electrical characteristics by employing microscale hierarchical structures. *ACS Nano*. 2014, **8**, 2959-2969, DOI: 10.1021/nn500257g.
33. Yang, W. L.; Liu, Y.; Hu, Y.; Zhou, M. J.; Qian, H. S. Microwave-assisted synthesis of porous CdO-CdS core-shell nanoboxes with enhanced visible-light-driven photocatalytic reduction of Cr(VI). *J. Mater. Chem*. 2012, **22**, 13895-13898, DOI: 10.1039/C2JM33010E.
34. Li, W.; Li, M. Y.; Xie, S. L.; Zhai, T.; Yu, M. H.; Liang, C. L.; Ouyang, X. W.; Lu, X. H.; Li, H. H.; Tong, Y. X. Improving the photoelectrochemical and photocatalytic performance of CdO nanorods with CdS decoration. *CrystEngComm*. 2013, **15**, 4212-4216, DOI: 10.1039/C3CE40092A.